Two-dimensional optical thermal ratchets based on Fibonacci spirals

Ke Xiao, Yael Roichman, and David G. Grier

Two-dimensional optical thermal ratchets based on Fibonacci spirals

Ke Xiao,[1] Yael Roichman,[2] and David G. Grier[1]

[1] *Department of Physics and Center for Soft Matter Research, New York University, New York, NY 10003*
[2] *School of Chemistry, Tel Aviv University, Tel Aviv, Israel 69978*
(Dated: June 24, 2011)

An ensemble of symmetric potential energy wells arranged at the vertices of a Fibonacci spiral can serve as the basis for an irreducibly two-dimensional thermal ratchet. Periodically rotating the potential energy landscape through a three-step cycle drives trapped Brownian particles along spiral trajectories through the pattern. Which spiral is selected depends on the angular displacement at each step, with transitions between selected spirals arising at rational proportions of the golden angle. Fibonacci spiral ratchets therefore display an exceptionally rich range of transport properties, including inhomogeneous states in which different parts of the pattern induce motion in different directions. Both the radial and angular components of these trajectories can undergo flux reversal as a function of the scale of the pattern or the rate of rotation.

Systems that rely on time-dependent forces to rectify thermal noise are called " thermal ratchets" [1–6]. Introduced with James Clerk Maxwell's thought experiments in the 1860's, thermal ratchets recently have enjoyed a resurgence of interest because of their relevance to biological molecular motors, and have been realized experimentally both for molecular [7, 8], micrometer-scaled [9–21] and for quantum objects [22]. Virtually all of these studies, however, have focused on one-dimensional systems [8–22], or on systems that can be projected onto one dimension [7, 21]. Comparatively little attention has been paid to thermal ratchets in two or higher dimensions.

The present study introduces an irreducibly two-dimensional thermal ratchet based on rotational symmetries of the Fibonacci spiral [23]. Section I presents the rich phenomenology of Fibonacci spiral ratchets comprised of discrete symmetric potential energy wells. This system features a deterministic regime in which the ratchet-induced flux spirals through the pattern of traps, and a stochastic regime in which diffusion-assisted transport admits flux reversals in both the radial and azimuthal degrees of freedom. These predictions are tested in Sec. II through experiments on colloidal spheres diffusing in water through rotating arrays of holographic optical traps arranged on the vertexes of Fibonacci spirals.

I. FIBONACCI SPIRAL RATCHET

A. Fibonacci spiral

The Fibonacci spiral [23] is a set of points in the plane whose n-th member falls at polar coordinates

$$r_n = R_0\, n^{\frac{1}{2}} \quad \text{and} \tag{1}$$
$$\theta_n = n\, \theta_0 \tag{2}$$

for $n = 0, 1, 2, \ldots$. It differs from a more general Archimedean spiral both by the square-root increase in radius and also by the choice of the Golden angle

$$\theta_0 = \frac{2\pi}{\phi^2}, \tag{3}$$

for the inter-node angular separation, where

$$\phi = \frac{\sqrt{5}+1}{2} = 1.6180339\ldots \tag{4}$$

is the irrational number known as the Golden mean. A typical example is plotted in Fig. 1. The overall scale factor R_0 does not enter into the definition of a Fibonacci spiral but plays a crucial role in its operation as a thermal ratchet.

This particular set of points is the densest packing of identical circles within a circular region [24]. As a result, it appears with great regularity in natural systems, most famously in the distribution of seeds within the seed-heads of sunflowers [25, 26].
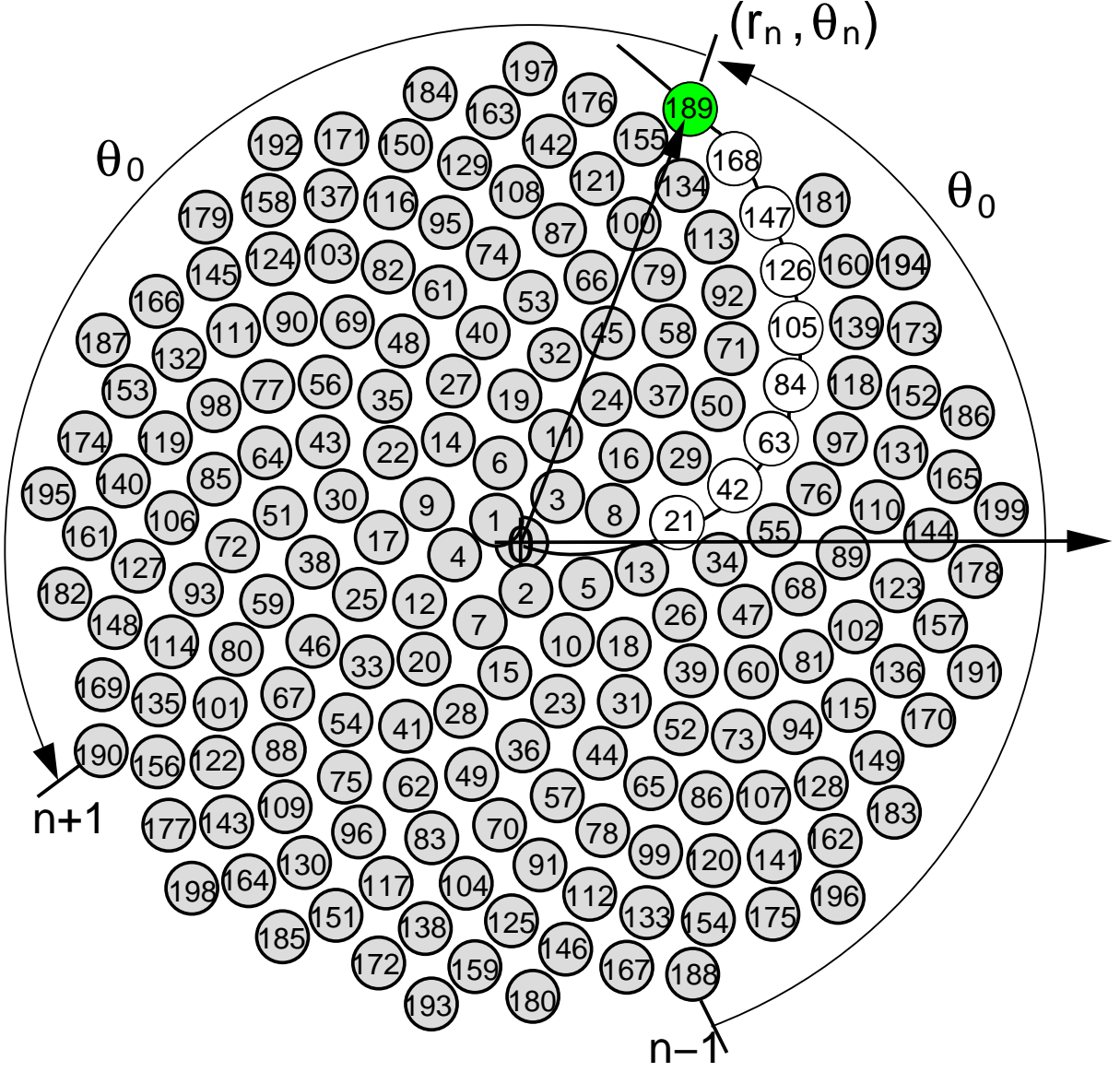
FIG. 1: Fibonacci spiral with vertexes labeled by index number n. The unshaded circles indicate the 21-st order of parastichies.

The dense packing of nodes in a Fibonacci spiral gives rise to a host of intriguing symmetries not found in other space-filling two-dimensional patterns. The principal Fibonacci spiral is defined by Eqs. (1) and (4) for integers n separated by unity. Higher-order spirals appear within this pattern for sequences of n that increase by steps equal to one of the Fibonacci numbers, F_m, which are defined recursively by $F_m = F_{m-1} + F_{m-2}$ [25, 27]. No other integers define regular spirals within the underlying pattern. The Fibonacci numbers also are noteworthy because their ratio approaches the Golden mean in the limit of large index, $\lim_{m \to \infty} F_{m+1}/F_m = \phi$.

Within a Fibonacci spiral, the m-th Fibonacci number, F_m, defines a set of F_m intertwined spirals, which have come to be known in the botanical context as *parastichies* of order F_m [28]. By definition, the F_m-th parastichy appears for radii $r > R_0 F_m^{1/2}$. Which parastichies are available at a given radius substantially influences the behavior of thermal ratchets based on Fibonacci spirals.
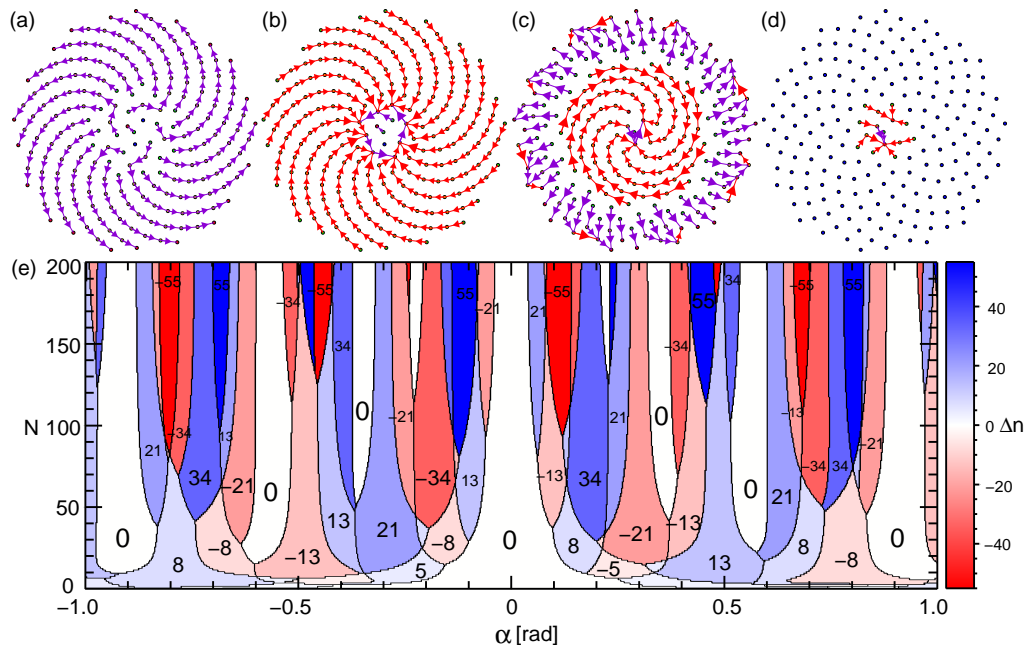
FIG. 2: (Color online) Transport in the three-state Fibonacci spiral ratchet. (a) $\alpha = -0.306$ rad, (b) $\alpha = 0.306$ rad, (c) $\alpha = 0.8$ rad, (d) $\alpha = 0.9$ rad. Arrows indicate direction of motion. (e) Displacement diagram as a function of the number of vertices N and the angle of rotation α. Numbers refer to the order of the parastichies along which particles travel for a given set of conditions, with positive numbers referring to outward motion. The domain for selecting each parastichy is shaded according to its Fibonacci number.

B. Three-state ratchet

We define a Fibonacci spiral ratchet by placing a spatially symmetric potential energy well of width σ at each vertex in the Fibonacci spiral. The resulting potential energy landscape is transformed into a ratchet potential through its time evolution. To break spatio-temporal symmetry we adopt the three-state protocol introduced originally for studies of one-dimensional ratchets [18, 29]. Rather than translating the pattern, as in earlier studies [18, 19, 29], we rotate it about its center:

$$\theta_n(t) = n\theta_0 + f(t), \tag{5}$$

with time depedence

$$f(t) = \begin{cases} 0, & 0 \le (t \bmod 3T) < T \\ \alpha, & T \le (t \bmod 3T) < 2T \\ 2\alpha, & 2T \le (t \bmod 3T) < 3T \end{cases} . \tag{6}$$

This cyclic pattern has period $3T$ and holds the landscape stationary for the duration T of each state. For simplicity, we also choose identical angular steps α between the states. The arrangement of traps and the three-state time evolution define the Fibonacci spiral ratchet whose performance dependends on the three control parameters, R_0, α, and T.

C. Deterministic regime

To study transport properties arising purely from the ratchet's geometry, we first select R_0 to be small enough that no force-free region exists within the pattern. Any object released from a vertex in one state will be drawn into the nearest potential well (vertex) in the next state. Cycling through a sequence of discrete angular steps therefore causes the object to move from one site on the lattice to another, a process that may be represented as a mapping of the spiral onto itself. This mapping depends on the sequence of nearest-neighbor steps in the intermediate states, which is determined by the angle of rotation, α. In this deterministic regime we assume that diffusion may be ignored.

Defining trajectories through the rotating Fibonacci spiral therefore involves finding the index n_1 of the rotated site that is closest to the vertex n in the previous state. We use the notation

$$S(n,k) = r_n \exp\left(i\left(\theta_n + k\alpha\right)\right)$$
$$= R_0\sqrt{n}\exp\left(i\left(n\theta_0 + k\alpha\right)\right) \tag{7}$$

to represent the n-th site of the lattice in the k-th state ($k = 0, 1, 2$). With this definition, the inter-vertex distance between the n-th site in the initial state and the n_1-th site after one step is

$$\Delta_{n,n_1}(\alpha) = |S(n,0) - S(n_1,1)|$$
$$= R_0\sqrt{n + n_1 - 2\sqrt{nn_1}\cos\left((n_1 - n)\theta_0 + \alpha\right)}. \tag{8}$$

We assume that a particle initially at site n will advance to the site n_1 whose index minimizes $\Delta_{n,n_1}(\alpha)$. Repeating the process for the second and third rotations yields the trajectory $n \to n_1 \to n_2 \to n'$. After one complete cycle, therefore, a particle initially at site n undergoes a change of index

$$\Delta n(n,\alpha) = n' - n. \tag{9}$$

The single-cycle mapping $\Delta n(n, \alpha)$ can be composed into trajectories that particles will follow through the array as the pattern cycles repeatedly through its sequence of states. Empirically, we observe that $\Delta n(n,\alpha)$ only takes on values $\pm F_m$ related to the Fibonacci numbers, and consequently that particles are conveyed along parastichies by the three-state ratchet cycle. Four examples are plotted in Fig. 2(a) through (d). Arrows in these plots indicate the direction of motion, with red traces indicating outward motion ($\Delta n > 0$) and blue indicating inward motion ($\Delta n < 0$). Trajectories characterized by large jumps in index are possible only for sufficiently large radii. Consequently, different parasticies may be selected at different radii within the spiral.

Figure 2(e) shows which trajectory is selected as a function of rotation angle α and radius within the spiral. Depending on the angular step, α, trajectories spiral inward or outward, clockwise or counterclockwise. In some cases, such as Fig. 2(d), there is no motion at all, $\Delta n(n,\alpha) = 0$. Each domain in Fig. 2(e) is labeled according to the parastichy Δn along which particles travel, with positive numbers indicating trajectories that spiral outward. The direction of motion also is indicated by the domains' shading.

The number of accessible domains increases in Fig. 2(e) as the number N of nodes in the spiral increases and additional Fibonacci numbers become accessible. Consequently, the selected parastichy tends to change with radius for all $\Delta n \neq 0$. This behavior is evident in Fig. 2(b), whose inner region spirals outward, and whose outer region spirals inward. The only exception arises for particular rotation angles

$$\alpha_0(m) = F_m\theta_0 - 2\pi F_{m-2}, \quad (m \geq 2). \tag{10}$$

which correspond to motionless states, $\Delta n = 0$.

The deterministic Fibonacci spiral ratchet thus exhibits far richer transport properties than any one-dimensional ratchet. This provides the foundation for the still more varied properties that arise when Fibonacci spiral is used as the basis for a thermal ratchet.

D. Stochastic regime

When R_0 is large enough that traps in consecutive states do not overlap, a Brownian particle released from a trap at the end of one state finds itself in a force-free region at the beginning of the next state. The particle can only advance through the pattern by diffusing. In one-dimensional ratchets, such a diffusive contribution to the transport process creates possibilities for temperature-dependent flux reversals [5, 18, 30]. Observing that particles travel along parastichies in the Fibonacci spiral ratchet's deterministic limit suggests that similar reversals should emerge in its stochastic limit. Unlike one-dimensional models, however, the stochastic limit of the Fibonacci spiral ratchet also can permit transport along directions not permitted in the deterministic limit.

To explore these possibilities, we model the trap at each vertex as a Gaussian potential well

$$V(\boldsymbol{r},t) = -V_0\sum_{n=1}^{N}\exp\left(-\frac{\left(\boldsymbol{r} - \boldsymbol{r}_n(t)\right)^2}{2\sigma^2}\right), \tag{11}$$
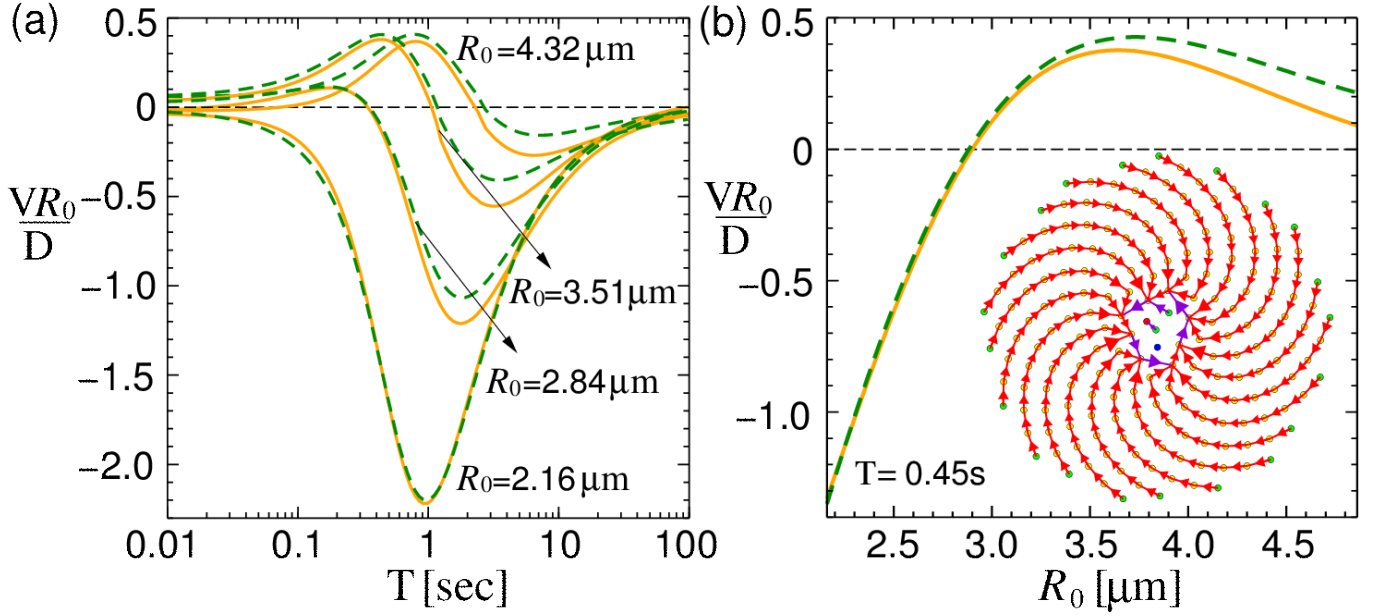
FIG. 3: (Color online) Flux calculated with Eqs. (11) through (15) in the radial (green dashed curve) and azimuthal (yellow solid curve) directions for the three-state Fibonacci spiral ratchet models for a particular angle of rotation, $\alpha = 0.306$ rad. (a) Flux as a function of state duration T for representative values of the pattern's scale, R_0. (b) Flux reversal as a function of scale for a fixed frequency of rotation, $T = 0.45$ sec. Inset: Deterministic map for $\alpha = 0.306$ rad.

where σ is the effective width of a trap, and V_0 is its depth. The time-evolution of the probability density $\rho(\boldsymbol{r}, t)$ for finding a particle at position $\boldsymbol{r}$ is described by the Fokker-Planck equation [31]

$$\frac{\partial \rho(\boldsymbol{r}, t)}{\partial t} = D \nabla^2 \rho(\boldsymbol{r}, t) - \mu \nabla \cdot [\rho(\boldsymbol{r}, t) \, \boldsymbol{F}(\boldsymbol{r}, t)], \tag{12}$$

where $\boldsymbol{F}(\boldsymbol{r}, t) = -\nabla V(\boldsymbol{r}, t)$, D is the particles' diffusion coefficient, and μ is their mobility. Equation (12) can be solved numerically using the finite-difference method [32] for any starting distribution $\rho(\boldsymbol{r}, 0)$. From this, the instantaneous local drift velocity induced by the ratchet potential can be computed as

$$\boldsymbol{v}(\boldsymbol{r}, t) = \mu \, \boldsymbol{F}(\boldsymbol{r}, t) - D \nabla \ln \rho(\boldsymbol{r}, t). \tag{13}$$

To characterize the ratchet's performance, we start with the traps occupied,

$$\rho(\boldsymbol{r}, 0) = \frac{1}{N} \sum_{n=1}^{N} \delta(\boldsymbol{r} - \boldsymbol{r}_n), \tag{14}$$

and compute the mean full-cycle velocity field

$$\bar{\boldsymbol{v}}(\boldsymbol{r}) = \frac{1}{3T} \int_0^{3T} \boldsymbol{v}(\boldsymbol{r}, t) \, dt. \tag{15}$$

This velocity field can be integrated to obtain trajectories that may be compared with the deterministic mapping. The same numerical model thus can be used to explore behavior in both the deterministic and stochastic regimes.

The results in Fig. 3 were computed for a particular choice of the rotation angle, $\alpha = 0.306$ rad, which corresponds to $\Delta n = -21$ in the deterministic limit. Deterministic trajectories wind clockwise and inward under these conditions, as indicated by the inset to Fig. 3(b). Other parameters were selected to mimic the experimental condition in Sec. II. The diffusion coefficient, $D = 0.3 \ \mu m^2/s$ is appropriate for 1.5 μm diameter spheres diffusing in water at room temperature, and corresponds to a mobility of $\mu = 73 \ \mu m/(pN \, s)$. The potential energy wells at each vertex were given a depth of $V_0 = 9 \ k_B T$ and a width of $\sigma = 0.75 \ \mu m$.

The results in Fig. 3(a) for the radial and azimuthal components of the induced drift velocity share much in common with results obtained from one-dimensional thermal ratchet models [18]. Traces in this figure show the drift velocity
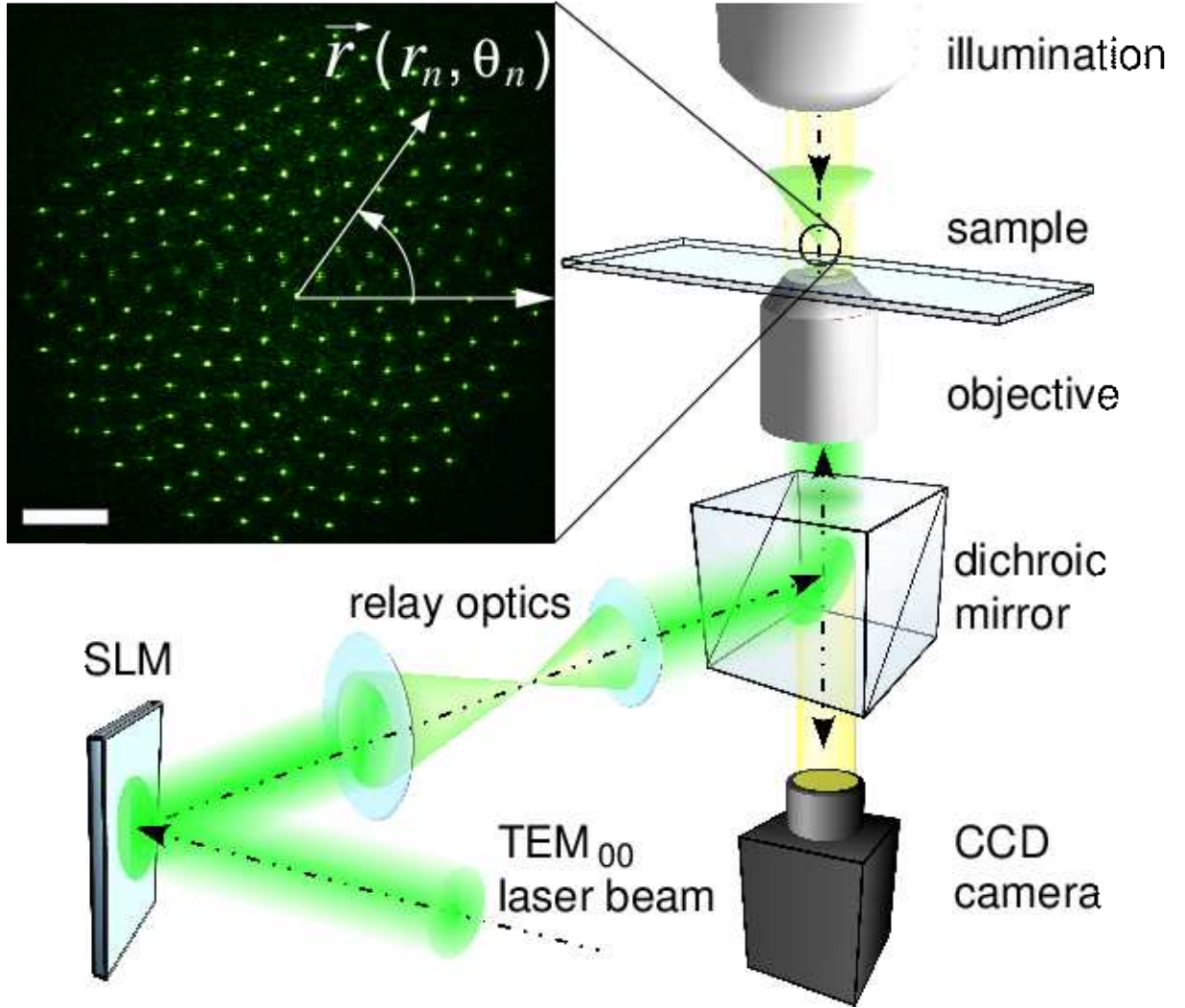
FIG. 4: (Color online) Schematic representation of an optical Fibonacci spiral ratchet implemented with holographic optical traps. Inset: Image of 200 optical traps arranged in a Fibonacci spiral. The coordinates of the nth trap (r_n, θ_n) is defined by Eq. (1). Scale bar indicates 10 μm.

normalized by the natural velocity scale, D/R_0, for a few representative values of the inter-trap separation, R_0. If the trapping pattern spends a long enough time T in each state, the diffusing particles fall preferentially into the nearest traps, and advance along the same trajectory as would have been selected deterministically. If, on the other hand, the pattern advances too rapidly, particles cannot reach the nearest trap in one time step. Rather, they preferentially find the nearest trap after two time steps, which carries them backward along the same path [18]. The drift velocity vanishes for large T because the pattern itself advances slowly. It vanishes for small T because the traps do not exert enough force to drag particles so quickly through the viscous medium.

Figure 3(b) shows how the radial and azimuthal components of the drift velocity depend on the scale of the pattern for a particular choice of T. Smaller-scale patterns favor transport along the deterministically selected direction. Larger inter-trap separations favor flux reversal by requiring particles to diffuse further between trapping events.

For a given state duration T, the flux also depends on the scale of the pattern, R_0. Smaller values of R_0 favor transport in the direction of the deterministic solution. Large values allow for flux reversal. This behavior can be seen in Fig. 3(b) at a fixed duration, $T = 0.45$ sec.

Both radial and azimuthal flux reversals resemble the single flux reversal observed in one-dimensional models [18]. Because the scale of the inter-trap separation along a parastichy depends on radius, however, flux may reverse in only part of the pattern for a given cycle time T. In a pattern-averaged sense, then, flux reversal in the radial and azimuthal direction need not occur at the same values of R_0 and T. Each flux reversal in the Fibonacci spiral thermal ratchet therefore can consist of two cross-overs. This is one respect in which this model differs from one-dimensional
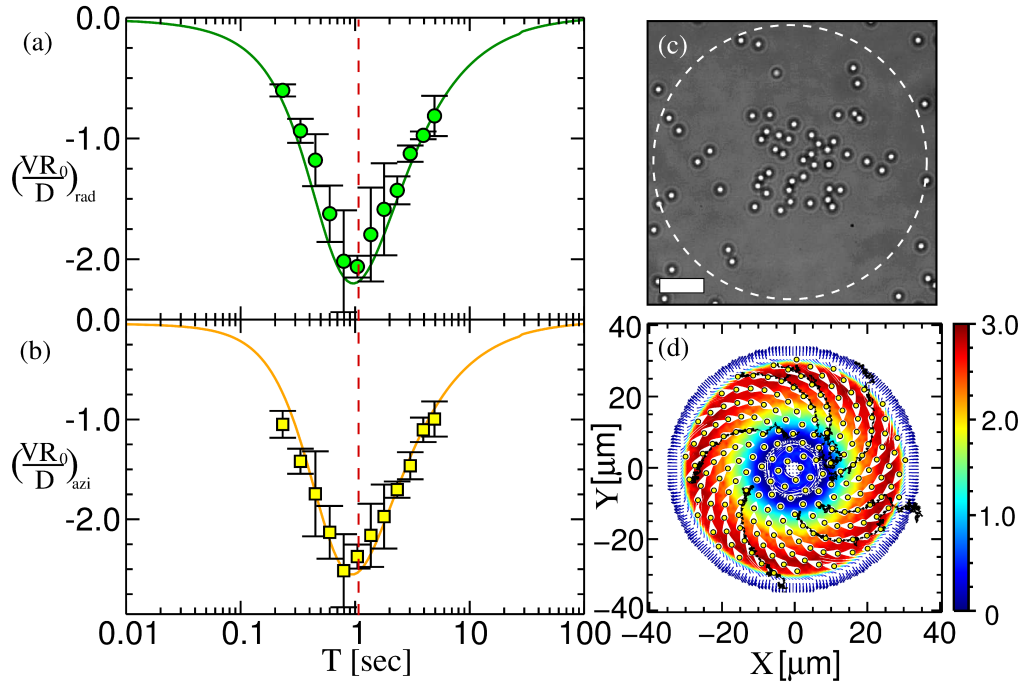
FIG. 5: (Color online) Flux measured in a three-state ratchet with 200 optical traps and $R_0 = 2.16$ μm for a fixed angle of rotation $\alpha = 0.306$ rad. (a) Radial flux from experimental data (circles) as a function of T. (b) Azimuthal flux from experimental data (squares) as a function of T. Solid curves in both (a) and (b) represent the numerical solutions of the Fokker-Planck equation. (c) Image of colloidal particles taken after 50 cycles with a optimal state duration $T = 1.06$ sec marked, as the vertical dashed line in (a) and (b). The dashed circle indicates the area subtended by the ratchet. Scale bar indicates 10 μm. (d) Representative experimental trajectories (black curves) for the optimal condition, plotted over streamlines of the computed velocity field, plotted as white barbs. In both cases, the experimentally observed trajectories follow the computed streamlines. Colors denote the computed speed in dimensionless units.

thermal ratchets.

Although computed for particular rotation angles, the results in Fig. 3 also highlight another general feature of transport in the Fibonacci spiral ratchet. Regardless of the size scale and cycle period, particles tend to follow the parastichy selected in the deterministic limit for the specific rotation angle, α.

II. EXPERIMENTAL DEMONSTRATION

We demonstrated both deterministic and stochastic modes of operation with experiments on colloidal spheres moving through holographically projected optical force landscapes. Our implementation is shown schematically in Fig. 4. The sample consists of 1.57 μm diameter colloidal silica spheres (Duke Scientific Catalog #8150, Lot #30158) dispersed in a 30 μm thick layer of water between a glass microscope slide and a glass coverslip. The edges of the sample volume were sealed with UV-cured adhesive (Norland Optical Adhesive Type 81) for mechanical stability and to slow evaporation. The sample was allowed to equilibrate to room temperature ($23 \pm 1°$C) on the stage of an inverted optical microscope (Nikon TE-2000U). Patterns of 200 optical tweezers arranged in a Fibonacci spiral according to Eqs. (1) through (4) were projected into the sample using the holographic optical trapping technique [33–37]. Computer-generated holograms [35] encoding the pattern of traps were imprinted onto the wavefronts of the trapping laser (Coherent Verdi 5W, 532 nm) using a liquid-crystal spatial light modulator (SLM; Hamamatsu X8267-16). Powering the hologram with 1.8 W provides each trap with an estimated 1.3 ± 0.3 mW, after accounting for the hologram's diffraction efficiency and other losses in the optical train. Each trap, therefore, has an estimated width of $\sigma = 0.85$ μm [38] and a depth of 9 $k_B T$ [39].

The microscope's objective lens (Nikon Plan-Apo 100×, numerical aperture 1.4, oil immersion) was used both to focus the traps into the sample, and also to image the spheres through conventional bright-field microscopy. Images were acquired with a low-noise monochrome video camera (NEC TI-324A II) at 30 frames per second with a spatial resolution of 0.135 μm per pixel. Individual particles were located in each snapshot to within 20 nm using standard
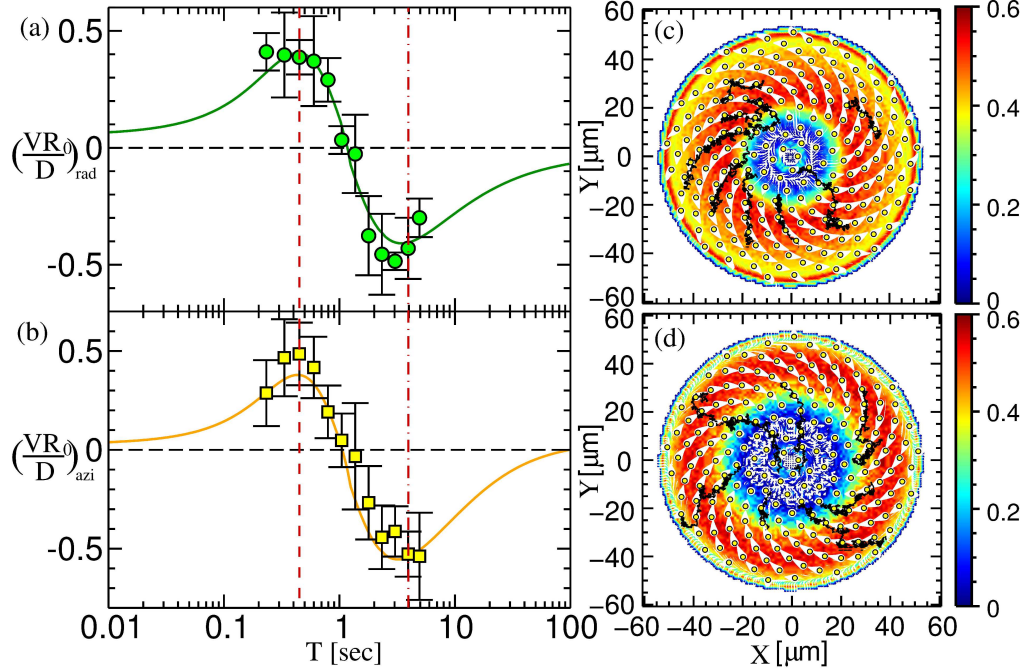
FIG. 6: Flux reversal measured in a three-state ratchet with 200 optical traps and $R_0 = 3.51$ μm for a fixed angle of rotation $\alpha = 0.306$ rad. (a) Radial flux from experimental data (circles) as a function of T. (b) Azimuthal flux from experimental data (squares) as a function of T. Solid curves in both (a) and (b) represent the numerical solutions of the Fokker-Planck equation. (c) and (d) Representative experimental trajectories (black curves) plotted over the numerically determined streamlines of the velocity field for $T = 0.45$ s and $T = 4.0$ s, respectively. Colors indicate the computed speed in dimensionless units.

methods of digital video microscopy [40]. Their locations were linked into time-resolved trajectories with a maximum likelihood algorithm [40]. These trajectories, in turn, were used to estimate the mean ratchet-induced flux using non-parametric density estimators [41]. The image of the focused traps inset into Fig. 4 was obtained by replacing the sample with a front-surface mirror.

The data in Fig. 5 show the radial and angular drift velocities measured for an optical Fibonacci spiral ratchet operating in the deterministic regime. The scale for the trapping pattern, $R_0 = 2.16$ μm, was selected to be small enough that traps overlap in consecutive states. The pattern was rotated according to Eq. (6) through an angle of $\alpha = 0.306$ rad by projecting a sequence of holograms with the SLM. The data in Fig. 5 were obtained by varying the duration T over which each hologram was projected. Each value represents the average of 1000 particles' trajectories measured over 80 cycles each. Any possible influence of out-of-plane fluctuations was minimized by projecting the traps at the spheres' equilibrium height above the wall [42]. The solid curves in Fig. 5 show results from numerical solutions of the Fokker-Planck equation, averaged over the entire pattern. Excellent agreement between simulation and experiment is obtained with no adjustable parameters.

As expected, no flux reversal occurs in this range of conditions. The induced drift vanishes as $1/T$ in the long-time limit. It also vanishes in the short-time limit because the traps do not exert enough force to move the particles so rapidly through the water. Over the entire range from $T = 0.2$ s to $T = 5$ s, the particles follow the trajectories predicted by the deterministic map in Fig. 3.

Increasing the scale of the trapping pattern to $R_0 = 3.51$ μm moves the system into the stochastic regime. Whereas the deterministic ratchet advected particles clockwise and inward along the $\Delta n = -21$ parastichy, the thermal ratchet admits flux reversal in both radial and azimuthal coordinates, as revealed in Fig. 6. The data for each T value in this plot were obtained from 2,000 particles' trajectories each consisting of 150 cycles. Substantially greater statistics are required in this case because the particles' drift is a comparatively small bias on their otherwise random trajectories. Even so, the ratchet-induced drift follows the deterministic map in the long-time limit. At shorter times, the drift velocity reverses direction, and particles run backward along the deterministically selected parastichy, The solid curves in Fig. 6(a) and (b) represent the numerical solutions of Eq. (12) and (15) for this set of conditions, again with no adjustable parameters. As in the deterministic limit, the optical Fibonacci spiral ratchet acts in quantitative agreement with theory when operated as a thermal ratchet.

Flux reversal occurs when the characteristic distance, $L = 2\sqrt{DT}$, that a particle diffuses during one step of the three-step cycle is smaller than one third of the distance between traps on the deterministically selected parastichy. This distance, however, is obtained from Eq. (9) and depends nontrivially on position within the spiral. Unlike a one-dimensional thermal ratchet, therefore, flux reversal can arise at different cycle times T at different radii within a Fibonacci spiral ratchet.

These experiments were carried out with 40 or fewer particles interacting with the trap array, or roughly 1 particle for every 5 traps. This occupation number appears to be small enough for quantitative agreement with the single-particle theory in Eqs. (11) through (15). Collisions arising in more highly occupied patterns could give rise to additional transport phenomena such as cooperative flux reversal of the type that is observed in ratchets for magnetic flux quanta [43, 44] and bacterial swarms [45]. This is a matter for future study.

III. CONCLUSIONS

We have demonstrated that the Fibonacci spiral can serve as the basis for a two-dimensional thermal ratchet model, and have implemented this model experimentally using colloidal spheres and holographic optical traps. Periodically rotating a spiral trapping pattern through a three-state sequence causes diffusing particles to drift both radially and azimuthally. The speed and direction of the ratchet-induced motion have a very rich dependence on the scale, R_0, of the pattern and on the angle α of the rotation. Remarkably, this seemingly complex dynamical system follows comparatively simple rules, with particles flowing along well-defined paths through the pattern that are selected principally by α for a given radius within the pattern. Varying R_0 and the cycle time T affords control over the rate and direction of motion along these paths.

The transition to flux-reversed transport need not occur uniformly within the Fibonacci spiral. Rather, some regions may follow the deterministic route while others flow in a retrograde direction. This creates the possibility that the system-averaged flux may undergo radial flux reversal separately from angular flux reversal.

[1] M. O. Magnasco, Phys. Rev. Lett. **71**, 1477 (1993).
[2] J. Prost, J. F. Chauwin, L. Peliti, and A. Ajdari, Phys. Rev. Lett. **72**, 2652 (1994).
[3] F. Jülicher, A. Ajdari, and J. Prost, Rev. Mod. Phys. **69**, 1269 (1997).
[4] R. D. Astumian and P. Hänggi, Physics Today **55**, 33 (2002).
[5] P. Reimann, Phys. Rep. **361**, 57 (2002).
[6] H. Linke, Appl. Phys. A **75**, 167 (2002).
[7] A. van Oudenaarden and S. G. Boxer, Science **285**, 1046 (1999).
[8] J. V. Hernández, E. R. Key, and D. A. Leigh, Science **306**, 1532 (2004).
[9] J. Rousselet, L. Salome, A. Ajdari, and J. Prost, Nature **370**, 446 (1994).
[10] L. P. Faucheux and A. Libchaber, J. Chem. Soc. Faraday Trans. **91**, 3163 (1995).
[11] L. Gorre-Talini, S. Jeanjean, and P. Silberzan, Phys. Rev. E **56**, 2025 (1997).
[12] L. Gorre-Talini, J. P. Spatz, and P. Silberzan, Chaos **8**, 650 (1998).
[13] J. S. Bader, R. W. Hammond, S. A. Henck, M. W. Deem, G. A. McDermott, J. M. Bustillo, J. W. Simpson, G. T. Mulhern, and J. M. Rothberg, Proc. Nat. Acad. Sci. **96**, 13165 (1999).
[14] L. P. Faucheux, L. S. Bourdieu, P. D. Kaplan, and A. J. Libchaber, Phys. Rev. Lett. **74**, 1504 (1995).
[15] L. P. Faucheux, G. Stolovitzky, and A. Libchaber, Phys. Rev. E **51**, 5239 (1995).
[16] L. I. McCann, M. Dykman, and B. Golding, Nature **402**, 785 (1999).
[17] M. I. Dykman, B. Golding, L. I. McCann, V. N. Smelyanskiy, D. G. Luchinsky, R. Manella, and P. V. E. McClintock, Chaos **11**, 587 (2001).
[18] S.-H. Lee, K. Ladavac, M. Polin, and D. G. Grier, Phys. Rev. Lett. **94**, 110601 (2005).
[19] S.-H. Lee and D. G. Grier, Phys. Rev. E **71**, 060102(R) (2005).
[20] S. Bleil, P. Reimann, and C. Bechinger, Phys. Rev. E **75**, 031117 (2007).
[21] S.-H. Lee and D. G. Grier, J. Phys.: Condens. Matter **17**, S3685 (2006).
[22] H. Linke, T. E. Humphrey, A. Löfgren, A. O. Sushkov, R. Newbury, R. P. Taylor, and P. Omling, Science **286**, 2314 (1999).
[23] H. Vogel, Mathematical Biosciences **44**, 179 (1979).
[24] J. N. Ridley, Mathematical Biosciences **58**, 129 (1982).
[25] R. O. Erickson, *The geometry of phyllotaxis* (Cambridge University Press, New York, 1983).
[26] R. V. Jean, Mathematical Biosciences **64**, 1 (1983).
[27] A. M. Mathai and T. A. David, Mathematical Biosciences **20**, 117 (1974).
[28] G. J. Mitchison, Science **196**, 270 (1977).
[29] B. A. Koss and D. G. Grier, Appl. Phys. Lett. **82**, 3985 (2003).

[30] J.-F. Chauwin, A. Ajdari, and J. Prost, Europhys. Lett. **32**, 373 (1995).

[31] H. Risken, *The Fokker-Planck Equation*, Springer series in synergetics (Springer-Verlag, Berlin, 1989), 2nd ed.

[32] J. C. Strikwerda, *Finite Difference Schemes and Partial Differential Equations* (SIAM, Philadelphia, 2004), 2nd ed.

[33] E. R. Dufresne and D. G. Grier, Rev. Sci. Instrum. **69**, 1974 (1998).

[34] E. R. Dufresne, D. Altman, and D. G. Grier, Europhys. Lett. **53**, 264 (2001).

[35] M. Polin, K. Ladavac, S.-H. Lee, Y. Roichman, and D. G. Grier, Opt. Express **13**, 5831 (2005).

[36] Y. Roichman, A. S. Waldron, E. Gardel, and D. G. Grier, Appl. Opt. **45**, 3425 (2006).

[37] D. G. Grier, Nature **424**, 810 (2003).

[38] K. Ladavac, K. Kasza, and D. G. Grier, Phys. Rev. E **70**, 010901(R) (2004).

[39] K. Xiao and D. G. Grier, Phys. Rev. Lett. **104**, 028302 (2010).

[40] J. C. Crocker and D. G. Grier, J. Colloid Interface Sci. **179**, 298 (1996).

[41] B. W. Silverman, *Density Estimation for Statistics and Data Analysis* (Chapman & Hall, New York, 1992).

[42] S. H. Behrens, J. Plewa, and D. G. Grier, Euro. Phys. J. E **10**, 115 (2003).

[43] J. E. Villegas, S. Savel'ev, F. Nori, E. M. Gonzalez, J. V. Anguita, R. García, and J. L. Vicent, Science **302**, 1188 (2003).

[44] C. C. de Souza Silva, J. van de Vondel, M. Morelle, and V. V. Moshchalkov, Nature **440** (2006).

[45] G. Lambert, D. Liao, and R. H. Austin, Phys. Rev. Lett. **104**, 168102 (2010).